Poultry Science®

Whole-transcriptome sequencing reveals a melanin-related ceRNA regulatory network in the breast muscle of Xichuan black-bone chicken

Ruiting Li,[*,†,1] DongHua Li,[*,†,1,2] Shuohui Xu,[*,†] Pengwei Zhang,[*,†] Zhiyuan Zhang,[*,†] Fumin He,[*,†] Wenting Li,[*,†,‡] Guirong Sun,[*,†,‡] Ruirui Jiang,[*,†] Zhuanjian Li,[*,†] Yadong Tian,[*,†] Xiaojun Liu,[*,†] and Xiangtao Kang[*,†,‡]

[*]*College of Animal Science and Technology, Henan Agricultural University, Zhengzhou, 450046, China;* [†]*Henan Key Laboratory for Innovation and Utilization of Chicken Germplasm Resources, Zhengzhou, 450046, China; and* [‡]*The Shennong Laboratory, Zhengzhou, 450046, China*

ABSTRACT The economic losses incurred due to reduced muscle pigmentation highlight the crucial role of melanin-based coloration in the meat of black-bone chickens. Melanogenesis in the breast muscle of black-bone chickens is currently poorly understood in terms of molecular mechanisms. This study employed whole-transcriptome sequencing to analyze black and white breast muscle samples from black-bone chickens, leading to the identification of 367 differentially expressed **(DE)** mRNAs, 48 DElncRNAs, 104 DEcircRNAs, and 112 DEmiRNAs involved in melanin deposition. Based on these findings, a competitive endogenous RNA (**ceRNA**) network was developed to better understand the complex mechanisms of melanin deposition. Furthermore, our analysis revealed key DEmRNAs (*TYR, DCT, EDNRB, MLPH* and *OCA2)* regulated by DEmiRNAs (g*ga-miR-140-5p, gga-miR-1682, gga-miR-3529, gga-miR-499-3p, novel-m0012-3p, gga-miR-200b-5p, gga-miR-203a, gga-miR-6651-5p, gga-miR-7455-3p, gga-miR-31-5p, miR-140-x, miR-455-x, novel-m0065-3p, gga-miR-29b-1-5p, miR-455-y, novel-m0085-3p, and gga-miR-196-1-3p).* These DEmiRNAs competitively interacted with DElncRNAs including *MSTRG.2609.2, MSTRG.4185.1, LOC112530666, LOC112533366, LOC771030, LOC107054724, LOC121107411, LOC100859072, LOC101750037, LOC121108550, LOC121109224, LOC121110876,* and *LOC101749016*, as well as DEcircRNAs, such as *novel_circ_000158, novel_circ_000623, novel_001518,* and *novel_circ_003596.* The findings from this study provide insight into the mechanisms that regulate lncRNA, circRNA, miRNA, and mRNA expression in chicken melanin deposition.

Key words: melanin deposition, muscle, whole-transcriptome sequencing, ceRNA regulatory network, black-bone chicken

2024 Poultry Science 103:103539
https://doi.org/10.1016/j.psj.2024.103539

INTRODUCTION

The meat of black-boned chickens is highly regarded for its medicinal properties, which include not only immunity-enhancing (Yu et al., 2021) and weight control (Tu et al., 2009) effects but also activities against diseases such as diabetes (Lin et al., 2005; Tian et al., 2007). In the black-bone chicken market, muscle with a high melanin content is considered highly nutritious; therefore, meat color affects sensory quality and consumers' desire to buy. The degree of darkness in the muscle of a black-bone chicken is determined by the degree of melanin pigmentation in the chicken, which is produced by melanin bodies in melanocytes in the muscles (Haraszti et al., 2011). Therefore, it is crucial to understand how melanin is deposited in the muscles of black-boned chickens.

To date, studies related to muscle melanin in black-boned chickens have been limited to mRNA expression and metabolite content. Through transcriptome analysis of black and white chicken breast muscles, Yu successfully screened several key genes related to melanin production in chicken muscles, including premelanosome protein (**PMEL***), RAB29*, member RAS oncogene family (**RAB29***)*, and 5 solute vector superfamily genes (Yu et al., 2018). Li selected the breast muscle tissue of chickens fed tyrosine or not fed tyrosine for transcriptome sequencing and identified the genes *PMEL,* melanophilin *(***MLPH***)*, endothelin receptor B subtype 2 *(***EDNRB2***)*, and dopachrome tautomerase *(***DCT***)* as related to melanin deposition (Li et al., 2019). Li also characterized the

Received November 28, 2023.
Accepted February 5, 2024.

[1]Ruiting Li and DongHua Li are contributed equally to this work.

[2]Corresponding author: lidonghua6656@126.com

genome-wide breeding history-related features of black-bone chickens through combined whole-genome resequencing and transcriptome analysis and found that endothelin 3 (**EDN3**) generated black skin color by interacting with the upstream ncRNA *LOC101747896* (Li et al., 2020). Transcriptomic and metabolomic analyses revealed that the expression of the tyrosinase (**TYR**), tyrosinase related protein 1 (**TYRP1**), DOPAchrome tautomerase (**DOT**), premelanosome protein 17 (**PMEL17**), melan-A (***MLANA***), and PDZ domain containing 1 pseudogene 1 (**PDZK1**) genes was significantly upregulated in black breast muscle compared with white breast muscle (Dou et al., 2022). Although several genes associated with melanin deposition have been identified, the ceRNA regulatory network involved in melanin pigmentation in chicken muscle has not been defined. Studies have emphasized the complex interactions of noncoding RNAs, such as microRNAs (**miRNAs**), cyclic RNAs (**circRNAs**), and long noncoding RNAs (**lncRNAs**), in posttranscriptional regulatory networks (Ma et al., 2018; Wang et al., 2020).

The objective of this research study was to characterize the lncRNAs, circRNAs, miRNAs, and mRNAs expression patterns contributing to the regulation of chicken muscle melanin pigmentation. Additionally, we aimed to establish a ceRNA network, laying the foundation for subsequent studies on the mechanism underlying melanin pigmentation.

MATERIALS AND METHODS

Animals and Tissue Sampling

We obtained 6 female Xichuan black-bone chickens from the Henan Agricultural University's Poultry Germplasm Resource Farm, including 3 with black breast muscles (B1, B2, and B3) and 3 with white breast muscles (W1, W2, and W3) (Figure 1A). Three chickens in each group were euthanized at 1 d of age. The samples were then quickly preserved by freezing them in liquid nitrogen. The muscle tissue was fixed with a 4% paraformaldehyde solution and then embedded in paraffin sections. We used the Fontana–Masson Stain Kit (Legene, Beijing, China) for histochemical visualization of muscle melanin.

All animal-based experiments were carried out in compliance with the regulations and guidelines provided by the Institutional Animal Care and Use Committee (**IACUC**) of Henan Agricultural University, China. The study was approved under Permit Number 11-0085 on June 13, 2011.

RNA Isolation, Library Construction, and Sequencing

After extracting the total RNA from each sample, the 1% agarose gel electrophoresis was employed to evaluate

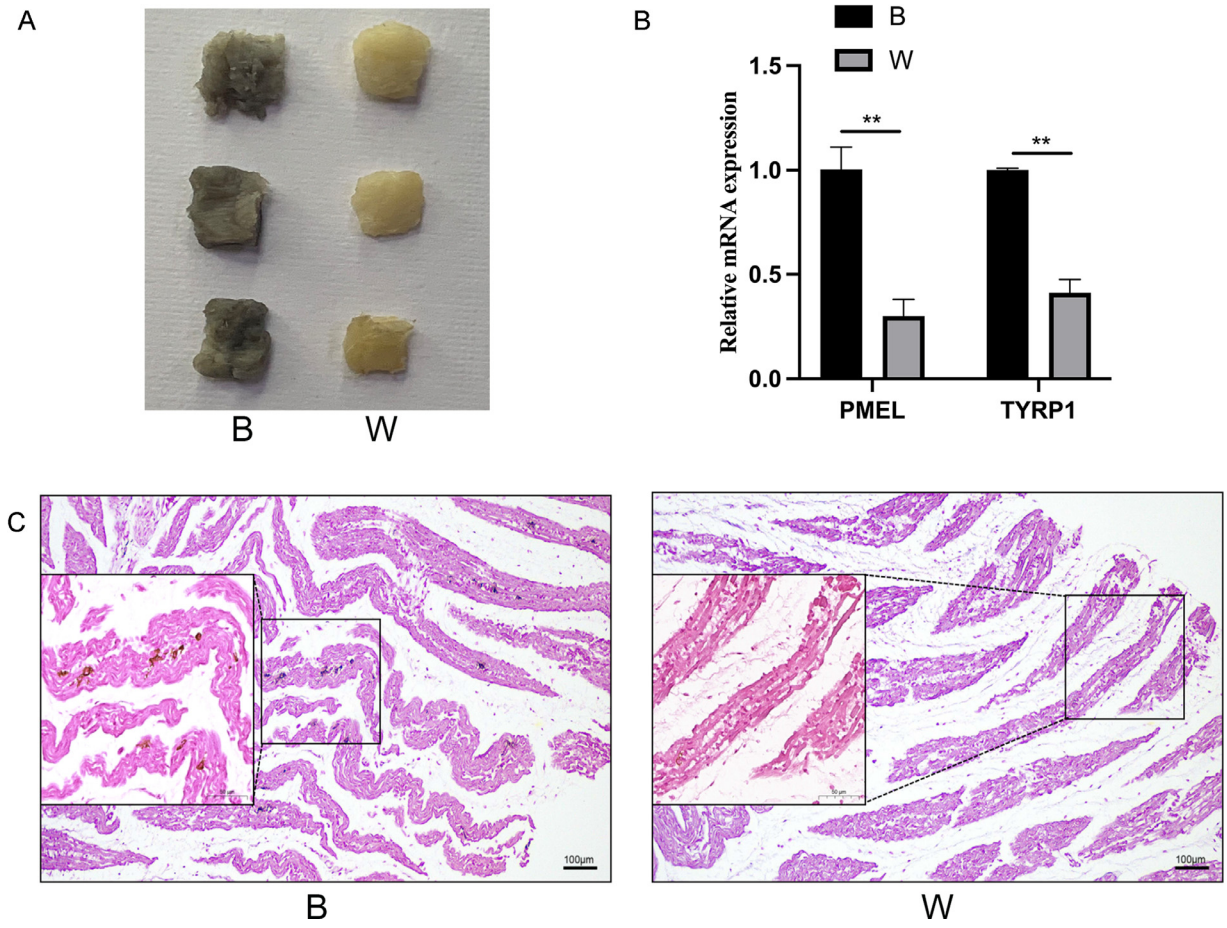

Figure 1. Differences in melanin deposition between black and white breast muscle. (A) Photographs of breast muscle sampled from 1-day-old Xichuan black-bone chickens. (B) Relative expression levels of *PMEL* and *TYRP1*. (C) Fontana–Masson staining of breast muscle, 100 × .

the quality of the RNA. Illumina's NEB Next Ultra RNA Library Prep Kit (New England Biolabs, Ipswich, MA, E7530) was utilized to construct 6 libraries of mRNA, lncRNA, and circRNA. The NEBNext Multiplex Small RNA Library Preparation Kit (E7300, NEB) was employed to generate the 6 miRNA sequencing libraries. Sequencing was performed on the resultant libraries utilizing an Illumina NovaSeq 6000 instrument (LC-BIO, Hangzhou, Zhejiang, China).

Screening for Differentially Expressed mRNAs

Reads with adapter contamination, low-quality bases, or bases that could not be detected were removed using Cutadapt (Kechin et al., 2017). A quality control tool was utilized to assess the quality of the sequences using the high-throughput sequence data provided by FastQC (http://www.bioinformatics.babraham.ac.uk/projects/fastqc/). After that, TopHat2 and Bowtie2 were employed to align the clean reads with the chicken reference genome GRCg7b (GCF_016699485.2), and StringTie was implemented to assemble the mapped reads (Langmead et al., 2012; Kim et al., 2013). Finally, Ballgown and StringTie were applied to assess the levels of expression for each transcript. DEmRNAs were described as those with mRNA false discovery rate (**FDR**) ≤ 0.05 and $|\log_2(\text{fold change})| > 1$ (Frazee et al., 2015; Pertea et al., 2015). The heatmaps were processed using the R package pheatmap. Blast2GO was utilized to conduct Gene Ontology (**GO**) term enrichment analysis with the GO database serving as the reference (Conesa et al., 2005). A Kyoto Encyclopedia of Genes and Genomes (**KEGG**) pathway analysis was performed by referring to the KEGG database (www.kegg.jp/kegg/kegg1.html) (Kanehisa et al., 2000). All terms with a P-value below 0.05 were determined to be significantly enriched.

lncRNA Identification and Analysis

The lncRNA transcriptome was constructed using StringTie (v1.3.1). Exon number (>2) and length (>200 nt) filters were applied to retain putative lncRNAs. To assess the coding ability of the putative lncRNAs, we utilized coding potential calculator 2 (**CPC2**) and coding non-coding index (**CNCI**) software, and candidate lncRNAs were identified by selecting the transcripts that were designated as having no coding potential according to both tools (Kang et al., 2017; Sun et al., 2013). To identify DElncRNAs, we applied the criteria $|\log_2(\text{fold change})| > 1$ and FDR < 0.05. Potential cis- and trans-target mRNAs of the DElncRNAs were identified by considering gene expression levels and chromosomal locations (Fu et al., 2019). DEmRNAs situated downstream and upstream of DElncRNAs by 100 kb were categorized as cis-acting target genes. Furthermore, the Pearson correlation coefficient was utilized to predict the extent of trans-regulation between genes and lncRNAs (Guil et al., 2012).

CircRNA Identification and Analysis

Initially, the clean data was aligned with the reference genome utilizing the BWA software (Houtgast et al., 2018). Moreover, a high-quality clean dataset was used to identify circRNAs using find_circ and Bowtie2. (Langmead et al., 2012). To analyze differential expression, raw counts were normalized by using **TPMs** (transcripts per million reads), and circRNAs with a $P < 0.05$ and $|\log_2(\text{fold change})| > 1$ were applied to the investigation of differential expression.

MiRNA Identification and Analysis

The distinct 16−35 nucleotide sequences were aligned using a BLAST search with species-specific precursors previously discovered in miRBase 21.0 (http://www.mirbase.org/) to facilitate the identification of novel and known miRNAs. TargetScan (version 7.0) and miRanda (v3.3a) were then combined with the differentially expressed miRNAs ($P < 0.05$ and $|\log_2(\text{fold change})| > 1$) across the black and white muscle libraries to determine the miRNA target genes (Agarwal et al., 2015).

CeRNA Network Construction and Analysis

TargetScan and MiRanda were utilized to predict miRNA-mRNA, miRNA-circRNA, and miRNA-lncRNA pairs. The Spearman correlation coefficient (**SCC**) was performed to assess the correlations between these pairs. Finally, a ceRNA network was established. Every regulatory network was visualized using Cytoscape v.3.2.1 software (Shannon et al., 2003).

Quantitative Real-Time Polymerase Chain Reaction (qRT-PCR) Validation

The LightCycler 96 instrument (Roche Applied Science, Indianapolis, IN) was employed to confirm 6 DEcircRNAs, DEmRNAs, DEmiRNAs, and DElncRNAs utilizing qRT-PCR with the SYBR Premix Ex Taq II Kit (TaKaRa). Glyceraldehyde-3-phosphate dehydrogenase (**GAPDH**) was utilized as the endogenous control for mRNAs, lncRNAs, and circRNAs. For miRNAs, U6 micronuclear RNA **(U6)** was used as an endogenous control. Table S1 displays the primer sequences developed with Oligo 6.0 software.

RESULTS

Differences in Melanin Deposition Between Black and White Muscle

After confirmation using qRT-PCR, it was shown that the black (**B**) group had higher melanin-associated gene expression *TYRP1* and *PMEL* compared to the white (**W**) group ($P < 0.05$) (Figure 1B). Additionally, Fontana−Masson staining of the breast muscle demonstrated some melanin pigment in group B but none in group W (Figure 1C). The findings revealed significant

phenotypic differences between the 2 experimental groups, which could be used to identify important circRNAs, miRNAs, mRNAs, and lncRNAs involved in the control of melanin pigmentation in chicken muscle.

Global Correlations of mRNAs with Melanin Deposition

The B and W libraries yielded 2,330, 4940, and 2,352,2282 clean reads, respectively, during whole-transcriptome sequencing of B1, B2, B3, W1, W2, and W3. A total of 11,080 mRNAs were identified in breast muscle after rigorous alignment with the chicken reference genome (Figure 2A). Of these genes, 367 DEmRNAs were identified, including 138 upregulated (37.60%) and 229 downregulated (62.40%) (Figure 2B). The expression profile of each group of DEmRNAs was visualized using a heatmap, and the DEmRNAs in the black and white breast muscles were found to be clustered separately (Figure 2C). Several genes that are crucial for melanin deposition were found among the DEmRNAs, such as *TYR, TYRP1, DCT,* endothelin receptor type B (**EDNRB**), *MLPH,* OCA2 melanosomal transmembrane protein (**OCA2**), *PMEL,* RAB38, member RAS oncogene family (**RAB38**), glycoprotein NMB (**GPNMB**), *MLANA,* cadherin 1 (**CDH1**) and solute carrier superfamily genes.

KEGG and GO analyses were carried out to investigate the roles of the DEmRNAs. Annotations for the majority of DEmRNAs included the following GO terms: The biological process (**BP**) includes "metabolic process," "single-organism process," and "cellular process"; cellular component (**CC**) includes "cell part," "cell," and "membrane"; and "binding", "transporter activity" and "catalytic activity" are classified as molecular functions (**MF**) (Figure 2D). The KEGG pathway enrichment results for DEmRNAs are illustrated in Figure 2E, which only includes the top 20 pathways with the smallest *P*-values. The following pathways exhibited a significant association with melanin: tyrosine metabolism *(TYR, TYRP1,* and *DCT),* phosphoenolpyruvate carboxykinase 1 (**PCK1**), muscarinic acetylcholine receptor M2 (**CHRM2**), thrombospondin 2 (**THBS2**), fibroblast growth factor receptor 2 (**FGFR2**), cartilage oligomeric matrix protein (**COMP**), laminin subunit alpha 1 (**LAMA1**), chondroadherin (**CHAD**), secreted phosphoprotein 1 (**SPP1**), tenascin (**TNC**), integrin binding sialoprotein (**IBSP**), integrin alpha 11 (**ITGA11**), collagen type IX alpha 1 chain (**COL9A1**), collagen type IX alpha 3 chain (**COL9A3**), DNA-damage-inducible transcript 4 (**DDIT4**) and thrombospondin 1 (**THBS1**). As per the findings of the gene set enrichment analysis (**GSEA**) software-based KEGG pathway enrichment analysis, tyrosine metabolism exhibited the highest degree of enrichment (Figure 2F).

Global Correlations of lncRNAs With Melanin Deposition

To identify lncRNAs, the RNA-seq data were matched to the reference chicken genome. During this alignment step, any reads corresponding to known lncRNAs were filtered out and excluded from subsequent analysis. The remaining reads were then subjected to analysis using CNCI and CPC2, which identified a total of 801 lncRNAs (Figure 3A). Among the DElncRNAs, 21 were upregulated, accounting for 43.75% of the total, while 27 DElncRNAs were downregulated, representing 56.25% of the total (Figure 3B). The overall patterns of expression for these DElncRNAs are shown in Figure 3C.

The expression of important genes can be controlled by lncRNAs via both cis- and trans-regulatory mechanisms. In this study, we did not find any cis-regulated lncRNAs but found a total of 48 trans-acting lncRNAs with 321 target genes. KEGG pathway analysis and GO annotation of the correlated target genes were carried out to get additional insight into the role of these trans-acting lncRNAs in the control of melanin deposition. Forty-four GO terms were employed to annotate the trans-targets of the DElncRNAs, with significant representation of BP categories including "Metabolic process," "single-organism process," and "cellular process"; MF categories including "transporter activity," "catalytic activity," and "binding"; and CC categories including "cell," "cell component," and "membrane" (Figure 3D). In addition, several pathways associated with melanin deposition, including the PI3K-Akt, tyrosine metabolism, and TGF-β signaling pathways, were found to be substantially enriched in the KEGG pathway analysis of the trans-targets regulated by the DElncRNAs (Figure 3E). In addition, many trans-target DEmRNAs, namely, *TYR, TYRP1, DCT,* and *EDNRB*, were also enriched in melanogenesis.

Global Correlations of CircRNAs With Melanin Deposition

A total of 4,870 circRNAs were detected, with 1,239 specific to black breast muscle and 1,162 specific to white breast muscle (Figure 4A). 104 DEcircRNAs were discovered in total as a result of the screening procedure. Among these DEcircRNAs, 53 were upregulated, 51 were downregulated, and the 104 DEcircRNAs we screened were derived from 94 host genes (Figure 4B). A heatmap was generated to visualize the clustering of DEcircRNAs between the 2 groups (Figure 4C). The DEcircRNA-hosting genes were examined by GO and KEGG enrichment methods to elucidate their activities in further detail. The majority of the DEcircRNA-hosting genes were found to be enriched in the cellular process, binding, and cell component, according to GO enrichment analysis (Figure 4D). Six KEGG pathways were found to be significantly enriched ($P < 0.05$) among the 63 KEGG pathways to which the DEcircRNA-hosting genes were annotated: endometrial cancer, arrhythmogenic right ventricular cardiomyopathy, the pentose phosphate pathway, the Hippo signaling pathway, adherens junctions, and bacterial invasion of epithelial cells (Figure 4E).

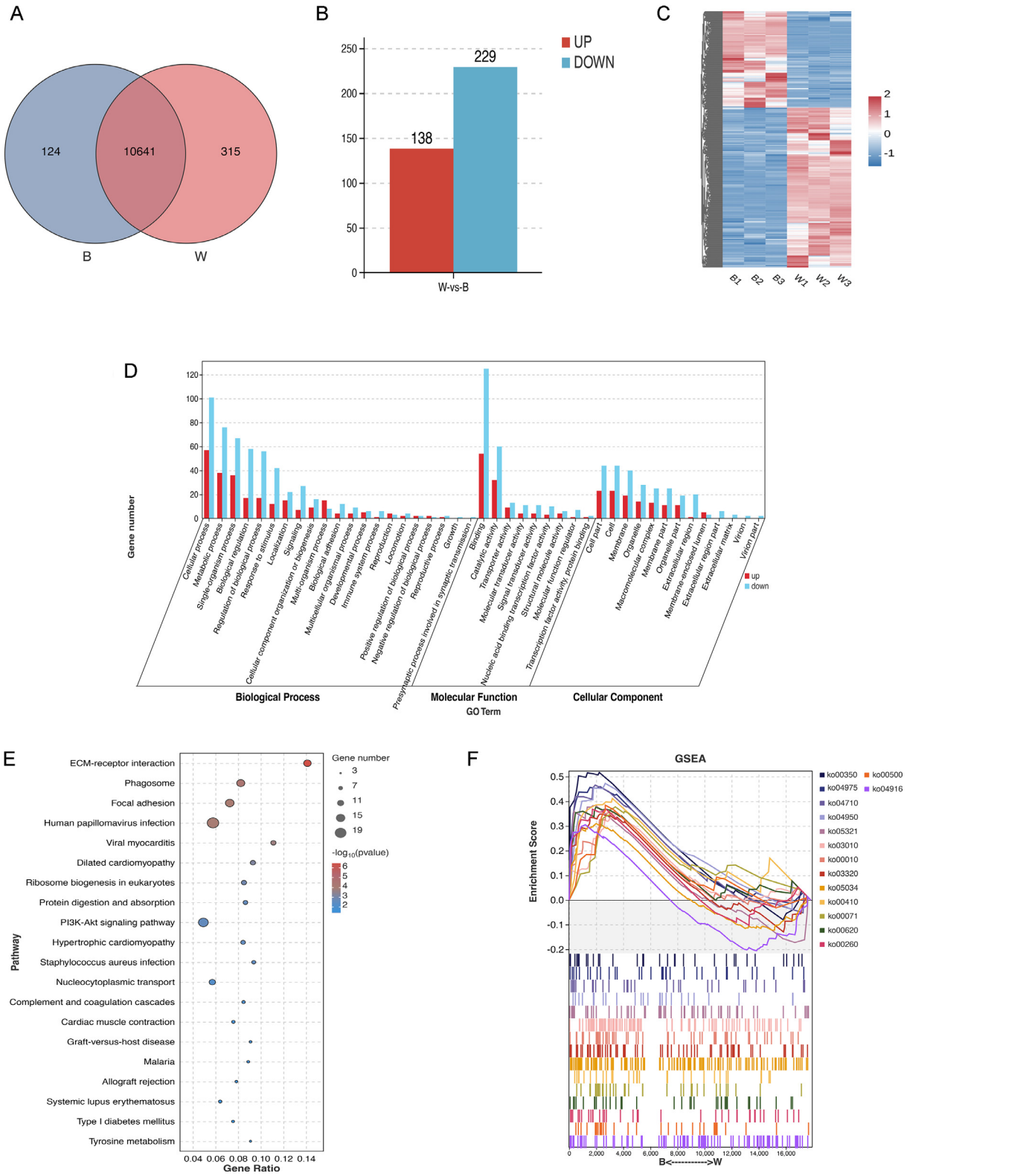

Figure 2. Analysis and identification of DEmRNAs between black and white breast muscle. (A) Venn diagram displaying the mRNA number; (B) Statistics on the number of down- and up-regulated DEmRNAs; (C) Heatmap of DEmRNA; (D) GO classification of DEGs; (E) A scatterplot representing the top 20 pathways based on KEGG enrichment.; (F) GSEA of KEGG.

Global Correlations of miRNAs With Melanin Deposition

The miRNA profile associated with melanin deposition in the breast muscle of black-bone chickens was examined using both sRNA libraries and sequencing. The black and white libraries yielded 32,387,496 and 32,348,875 clean reads, respectively, after filtering. The majority of the miRNA clean reads had lengths ranging from 21 to 24 bp, consistent with the typical characteristics of miRNAs. These findings further validate the reliability of our dataset (Figure 5A). In total, 550 miRNAs

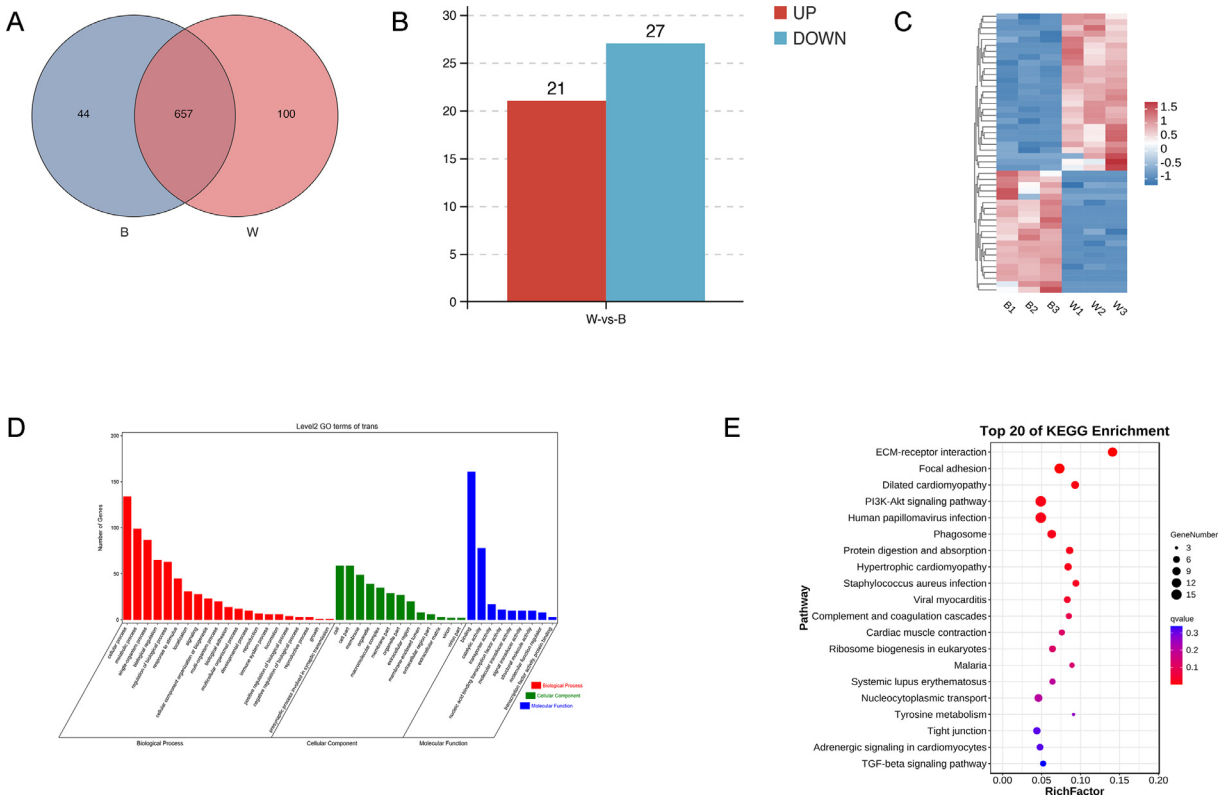

Figure 3. Analysis and identification of DElncRNAs between black and white breast muscle. (A) Venn diagram demonstrating the number of lncRNAs; (B) Statistics on the number of down- and up-regulated DElncRNAs; (C) Heatmap of DElncRNAs; (D) GO classification and (E) KEGG enrichment of trans-target genes regulated by DElncRNAs.

were detected, including 49 specific to black breast muscle and 30 specific to white breast muscle (Figure 5B). A total of 112 DEmiRNAs were found, of which 66 exhibited upregulation (58.93%) and 46 demonstrated downregulation (41.07%) in black muscle (Figure 5C). The DEmiRNA expression profiles of the samples are presented in Figure 5D.

For predicting DEmiRNA target genes, 2 prediction software programs were used: miRanda and TargetScan. A total of 256 DEmRNAs and 78 DEmiRNAs were

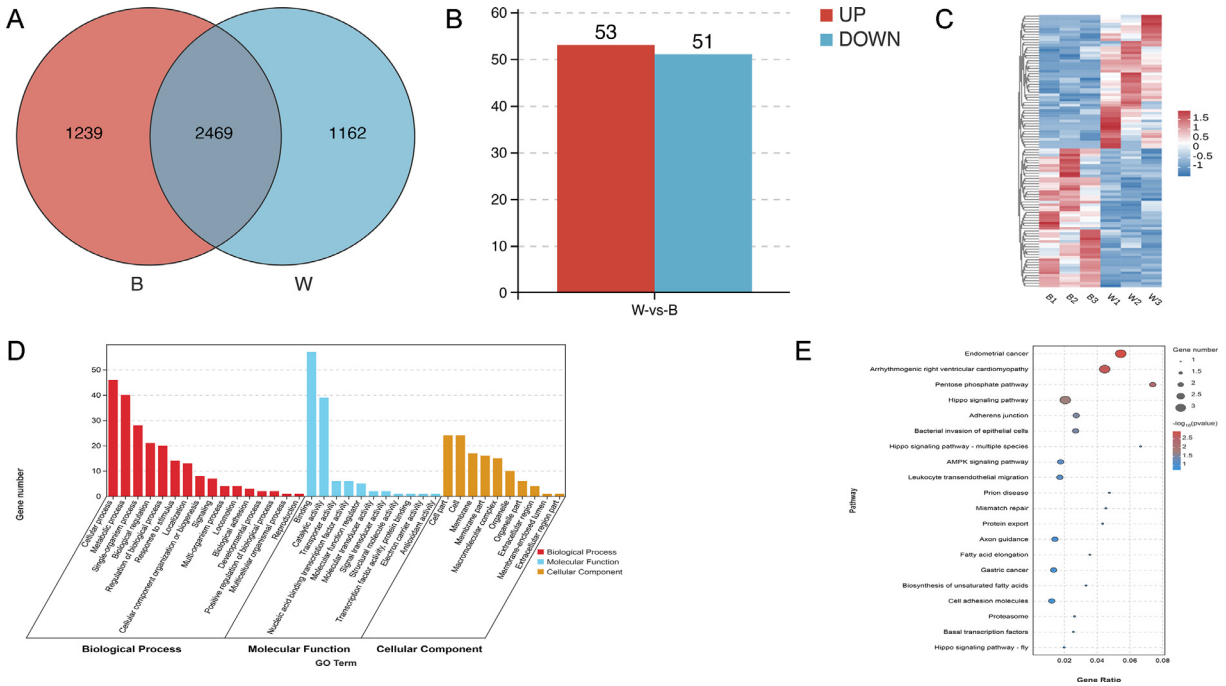

Figure 4. Analysis and identification of DEcircRNAs between black and white breast muscle. (A) Venn diagram illustrating the number of DEcircRNAs; (B) Statistics on the number of down- and up-regulated DEcircRNAs; (C) Heatmap of DEcircRNAs; (D) GO classification and (E) KEGG enrichment of DEcircRNA-hosting genes.

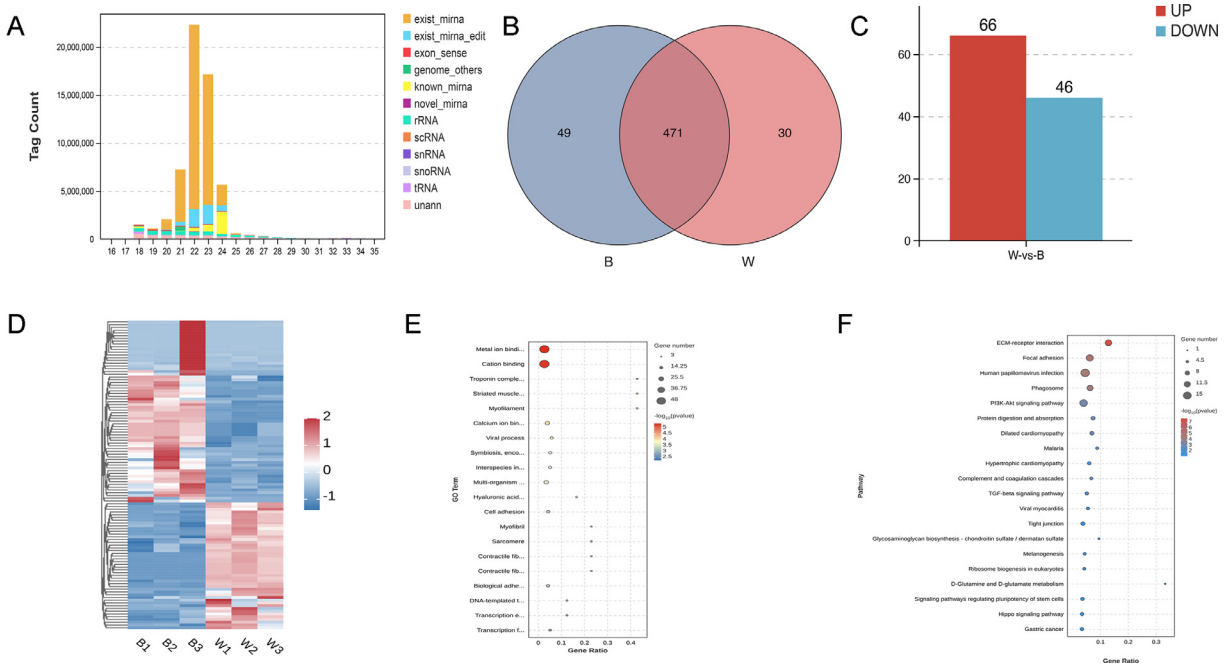

Figure 5. Analysis and identification of DEmiRNAs between black and white breast muscle. (A) Length distribution of small RNA reads. (B) Venn diagram illustrating the number of miRNAs; (C) Statistics on the number of down- and up-regulated DEmiRNAs; (D) Heatmap of DEmiRNAs; (E) GO enrichment and (F) KEGG enrichment of DEmiRNA target genes.

found to form 1124 miRNA–mRNA pairs. Out of 1,266 GO terms, 167 exhibited significant enrichment ($P < 0.05$) for DEmiRNA target genes. Metal ion binding, cation binding, and the troponin complex were the most significantly enriched (Figure 5E). KEGG enrichment analysis revealed 154 pathways among the target genes of the DEmiRNAs. Some of these pathways, including melanogenesis, PI3K-Akt signaling, and TGF-β signaling, are implicated in melanin deposition (Figure 5F).

qRT-PCR Validation of DEcircRNAs, DEmRNAs, DEmiRNAs, and DElncRNAs

For validation using qRT-PCR, a random selection of 24 transcripts was made from the DEcircRNAs, DEmRNAs, DEmiRNAs, and DElncRNAs. The expression patterns of these transcripts correlated with the RNA-seq data, indicating the accuracy of the RNA-seq results (Figure 6; Table S2).

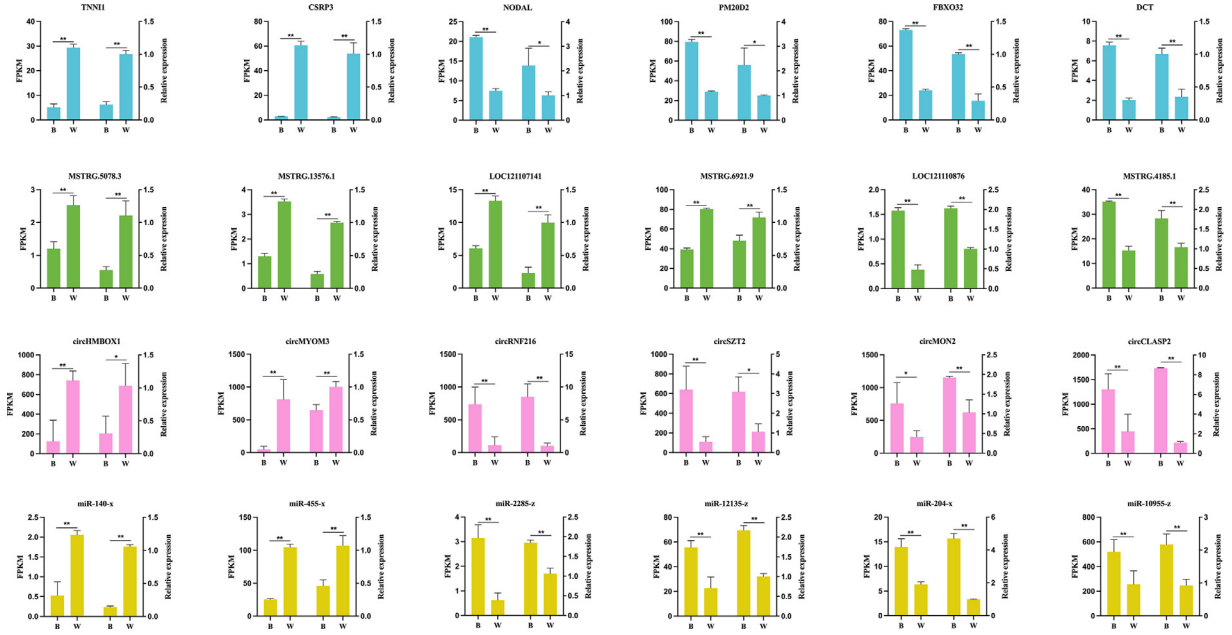

Figure 6. Validation of the RNA-seq findings using RT-qPCR. The Y-axis on the right represents the data from RT-qPCR, and the left Y-axis shows the FPKM values obtained from the RNA-seq data. The data are presented as the means ± SEDs. Whereas ** denotes $P < 0.01$ and * denotes $P < 0.05$.

Construction and Analysis of the ceRNA Regulatory Network

By screening the DElncRNAs, DEmRNAs, and DEcircRNAs that are regulated by the same DEmiRNAs in the DEmiRNA−DElncRNA, DEmiRNA−DEmRNA, and DEmiRNA−DEcircRNA regulatory relationships, we ultimately established 1001 circRNA−miRNA−mRNA and 8551 lncRNA−miRNA−mRNA interactions (Table S3). KEGG enrichment analyses were conducted to identify DEmRNAs associated with the DElncRNA/DEcircRNA−DEmiRNA−DEmRNA regulatory network (Figure 7). The results of the enrichment analyses indicated the presence of DEmiRNA, DElncRNA, and DEcircRNA-related genes, including *TYR, DCT*, and *EDNRB*, were strongly enriched in melanogenesis and tyrosine metabolism. Notably, although there was no significant enrichment of the Wnt signaling pathway according to the KEGG enrichment analysis (Table S4), we noted that several DEmRNAs were involved in this pathway, including leucine-rich repeat-containing G protein-coupled receptor 5 (**LGR5A**), R-spondin 4 (**RSPO4**), catenin delta-2 (**CTNND2**), and frequently rearranged in advanced T-cell lymphomas 2 (**FRAT2**). In addition, there were some DEmRNAs related to melanin deposition that were not annotated to any specific KEGG pathways, such as *MLPH* and *OCA2*, which also deserve attention. To further investigate the potential ceRNA−transcript relationships, we identified 5 known DEmRNAs *(TYR, DCT, EDNRB, MLPH,* and *OCA2)* related to chicken melanin deposition from the ceRNA networks. Finally, we established a ceRNA network including 13 DElncRNAs (*MSTRG.2609.2, MSTRG.4185.1, LOC112530666, LOC112533366, LOC771030, LOC107054724, LOC121107411, LOC100859072, LOC101750037, LOC121108550, LOC121109224, LOC121110876,* and *LOC101749016)*, 4 DEcircRNAs *(novel_circ_000158, novel_circ_000623, novel_circ_001518,* and *novel_circ_003596)*, 17 DEmiRNAs (*gga-miR-140-5p, gga-miR-1682, gga-miR-3529, gga-miR-499-3p, novel-m0012-3p, gga-miR-200b-5p, gga-miR-203a, gga-miR-6651-5p, gga-miR-7455-3p, gga-miR-31-5p, miR-140-x, miR-455-x, novel-m0065-3p, gga-miR-29b-1-5p, miR-455-y, novel-m0085-3p,* and *gga-miR-196-1-3p)*, 5 DEmRNAs *(TYR, DCT, EDNRB, MLPH,* and *OCA2)*, and 90 total interactions (Figure 8).

DISCUSSION

The ceRNA model has been widely accepted in recent years and used to explain various genetic mechanisms (Salmena et al., 2011; Ala et al., 2013). However, there have been no studies on the ceRNA network associated with melanin deposition in chicken breast muscles. In this study, comparisons of black and white breast muscle samples revealed 367 DEmRNAs, 48 DElncRNAs, 104 DEcircRNAs, and 112 DEmiRNAs. Based on these results, lncRNA/circRNA−miRNA−mRNA networks that potentially regulate melanin deposition were constructed.

The potential roles of DEmRNAs, the DEcircRNAs' host genes, and the DElncRNAs/DEmiRNAs target genes were investigated using KEGG analysis. Except for the host genes of the DEcircRNAs, most of the DEmRNAs overlapped with the set of target genes of the DElncRNAs and DEmiRNAs (Figure S1A). Furthermore, these overlapped genes were considerably enriched in melanin deposition-related KEGG pathways, including tyrosine metabolism and melanogenesis ($P < 0.05$)

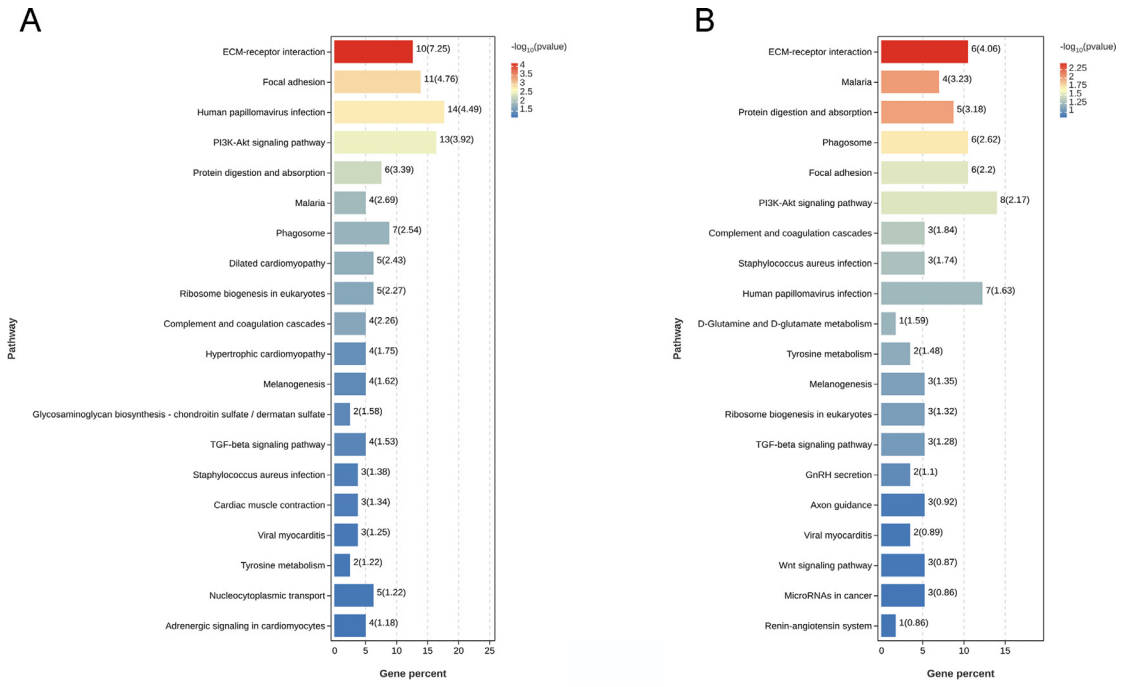

Figure 7. KEGG pathway enrichment analysis of the mRNAs involved in the ceRNA network revealed the top 20 enriched KEGG terms. (A) lncRNA−miRNA−mRNA network. (B) circRNA−miRNA−mRNA network.

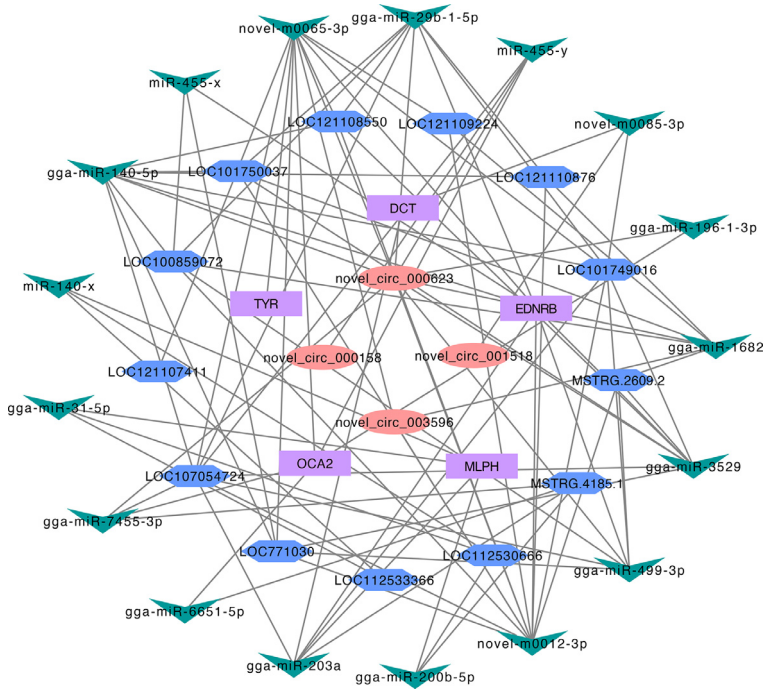

Figure 8. A ceRNA network was constructed with all the DEmRNAs, DElncRNAs, DEcircRNAs, and DEmiRNAs.

(Figure S1B). Interestingly, the obtained results are in line with the KEGG enrichment findings for DEmRNAs, the target genes of DElncRNAs/DEmiRNAs, and the DEmRNAs in the ceRNA network. Therefore, we speculate that the similarity of the sets of genes leads to the pathway similarity. Furthermore, these 2 pathways (tyrosine metabolism and melanogenesis), which are enriched among DEmRNAs and their associated ceRNAs, may be involved in melanin deposition.

Melanin production relies on the function of tyrosinase, which controls the rate of melanin synthesis (del Marmol et al., 1996; Lee et al., 2020). Many genes associated with melanin deposition, such as *TYR, TYRP1,* tyrosinase-related protein 2 (**TYRP2**), and *DCT*, are enriched in tyrosine metabolism pathways (Yuan et al., 2019; Dou et al., 2022; Kim et al., 2022). From our constructed ceRNA network, we identified 2 DEmRNAs (*TYR* and *DCT*) involved in tyrosine metabolism. *TYR* is known to be important for melanin production, and different *TYR* alleles have been reported to be related to the coloration of tissues such as skin, eyes, and feathers in various species (Stokowski et al., 2007; Park et al., 2016; Yang et al., 2019). In addition, *TYR* expression and activity can influence melanogenesis and the total cellular melanin content (Makpol et al., 2014; Paterson et al., 2015). *TYR* was found to be a target gene of *novel-m0065-3p* and to interact with *LOC121107411* and *novel_circ_003596*. DCT is an enzyme that is primarily involved in melanin synthesis in melanosomes and is a marker of melanocytes (Tímár et al., 2006; Pak et al., 2004). Moreover, *DCT* was significantly differentially expressed in the skin tissues of goats with different skin colors, indicating its possible regulatory effect on melanin deposition (Xiong et al., 2020). *DCT* was found to be a target gene of *gga-miR-203a* and to interact with *LOC101749016*, whereas *DCT* was a target gene of *novel-m0085-3p* and interacted with *LOC101749016* and *novel_circ_001518*. Melanogenesis is another pathway that affects melanin deposition. Melanogenesis is enriched in genes associated with melanin deposition, such as *EDNRB*, melanocortin 1 receptor (**MC1R**), and melanogenesis-associated transcription factor (**MITF**) (Jung et al., 2016; Pillaiyar et al., 2017; Wang et al., 2021). Based on our constructed ceRNA network, we determined that *EDNRB* was enriched in tyrosine metabolism. *EDNRB* and its endothelin ligand (**EDN**) play crucial roles in melanocyte development (Takeo et al., 2016). The signaling pathways associated with *EDNRB* are involved in promoting the proliferation, differentiation, and regeneration of melanocytes (Li et al., 2017). A ceRNA network study showed that *EDNRB* is involved in 68 networks with 9 DEmiRNAs (*gga-miR-140-5p, gga-miR-1682, gga-miR-3529, gga-miR-499-3p, novel-m0012-3p, miR-455-x, novel-m0065-3p, gga-miR-203a,* and *gga-miR-29b-1-5p*), 9 DElncRNAs (*MSTRG.2609.2, LOC771030, LOC107054724, LOC100859072, LOC101750037, LOC121108550, LOC121109224, LOC121110876,* and *LOC101749016*) and 2 DEcircRNAs (*novel_circ_000623* and *novel_circ_003596*).

Several DEmRNAs, such as *MLPH* and *OCA2*, were identified in the constructed ceRNA network. These genes were not shown to be enriched in melanin-related pathways, but previous studies have reported their association with melanin deposition (Dou et al., 2022). *MLPH* is involved in melanosome transport, and a growing number of findings suggest that polymorphisms within the *MLPH* gene are associated with coat color dilution in animals (Philipp et al., 2005; Ishida et al., 2006; Drögemüller et al., 2007). In the present study, *MLPH* targeted 2

DEmiRNAs (*gga-miR-200b-5p* and *gga-miR-203a*) and interacted with *MSTRG.4185.1*. In addition, *LOC112530666* may regulate *MLPH* by sponging 3 DEmiRNAs *(gga-miR-200b-5p, gga-miR-31-5p* and *miR-140-x*) to regulate melanin deposition. Notably, for the first time, we identified *OCA2* as affecting melanin content in chicken muscle. *OCA2* is a transmembrane protein found in the melanosome membrane. Numerous studies have suggested that this protein is involved in tyrosine transport and the regulation of melanosome pH and melanosome maturation (Rosemblat et al., 1994; Chen et al., 2002; Toyofuku et al., 2002). Genetic variations in *OCA2* are associated with skin pigmentation in humans and chickens (Edwards et al., 2010; Zi et al., 2023). In our study, *OCA2* was found to be regulated by 5 DEmiRNAs (*gga-miR-6651-5p, gga-miR-7455-3p, miR-455-y, novel-m0065-3p,* and *gga*-miR-196-1-3p) and to interact with *MSTRG.4185.1, LOC107054724, novel_circ_000158* and *novel_circ_000623*.

Melanin deposition is a multistage process involving melanocyte development, melanin synthesis, and melanosome transport. For the 5 genes discussed above (*TYR, DCT, EDNRB, MLPH,* and *OCA2*), we constructed a network of ceRNAs that function at various stages of melanin deposition (Figure 9). *MITF* is a transcription factor associated with microphthalmia that encodes multiple protein isomers, including *MITF-A, B, C, D, E, H, J, Mc, CM,* and *M*. Among them, *MITF-M* is the most abundant and is specifically expressed in melanocytes. *EDNRB* can phosphorylate the transcription factor *MITF* (Li et al., 2017). *MITF* not only regulates the development of melanocytes but also induces the expression of melanin-producing enzymes such as TYR, TYRP1, and DCT (Schiaffino, 2010). In melanosomes, DOPAchrome is synthesized from tyrosine through L-DOPA and L-DOPA quinone by the action of *TYR* (Shao et al., 2018). However, loss-of-function mutations in *OCA2* affect the conversion of tyrosine into L-DOPA (Protas et al., 2006). DOPAchrome is converted into 5,6-dihydroxyindole (**DHI**) and 5,6-dihydroxyindole-2-carboxylic acid (**DHICA**), which are then oxidatively polymerized to form eumelanin (Pralea et al., 2019), while *DCT* converts DOPAchrome to DHICA (Ng et al., 2009). Finally, melanosomes are transported to the cell membrane to distribute the melanin throughout the muscles (Wu et al., 2018). The "melanosome transport complex" is composed primarily of the RAB27A, member RAS oncogene family (**Rab27a)**, MLPH, and myosin-Va (**MyoVa)** proteins and is responsible for transporting melanosomes (Myung et al., 2021). Finally, the ceRNA network constructed from the 5 noteworthy DEmRNAs and their corresponding 13 DElncRNAs, 4 DEcircRNAs, and 17 DEmiRNAs was speculated to be related to melanin deposition in chicken breast muscle.

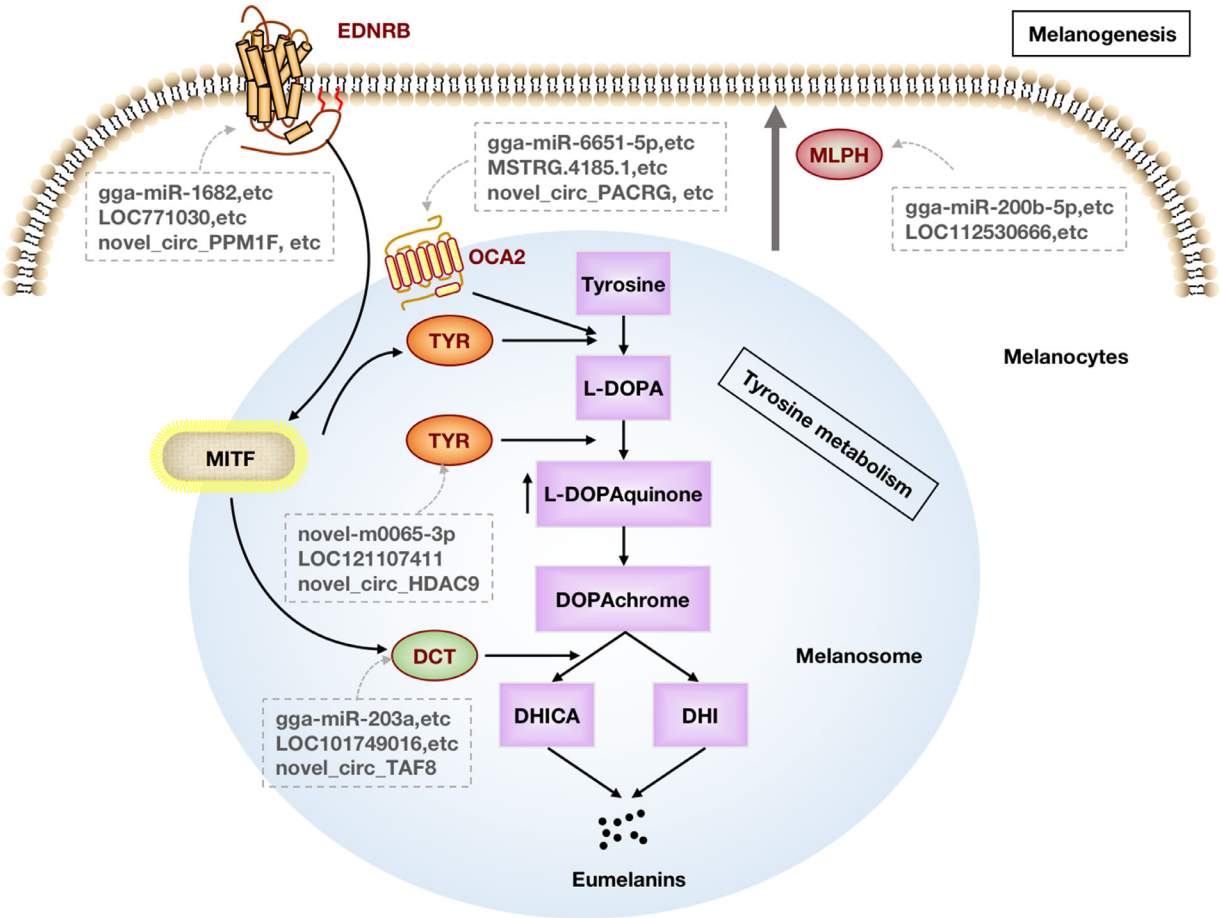

Figure 9. Mechanism of action of ceRNA networks during melanin deposition. Only the red letters represent DEmRNAs, and the gray letters represent DEcircRNAs, DEmiRNAs, and DElncRNAs in the ceRNA networks.

CONCLUSIONS

In this study, we constructed the first ceRNA network related to melanin deposition in the breast muscle of black-bone chickens, comprising 13 DElncRNAs *(MSTRG.2609.2, MSTRG.4185.1, LOC112530666, LOC112533366, LOC771030, LOC107054724, LOC121107411, LOC100859072, LOC101750037, LOC121108550, LOC121109224, LOC121110876,* and *LOC101749016)*, 4 DEcircRNAs *(novel_circ_000158, novel_circ_000623, novel_circ_001518,* and *novel_circ_003596)*, 17 DEmiRNAs *(gga-miR-140-5p, gga-miR-1682, gga-miR-3529, gga-miR-499-3p, novel-m0012-3p, gga-miR-200b-5p, gga-miR-203a, gga-miR-6651-5p, gga-miR-7455-3p, gga-miR-31-5p, miR-140-x, miR-455-x, novel-m0065-3p, gga-miR-29b-1-5p, miR-455-y, novel-m0085-3p,* and *gga-miR-196-1-3p)*, and 5 DEmRNAs *(TYR, DCT, EDNRB, MLPH* and *OCA2)*. This study provides a valuable resource for further characterizing the mechanisms underlying melanin deposition in black-bone chicken breast muscle and enhancing our understanding of the black-bone chicken transcriptome.

ACKNOWLEDGMENTS

This work was supported by the National Natural Science Foundation of China (32102540), the Zhongyuan Youth Postdoctoral Innovative Talent Project (ZYYCYU202012178), the China Agriculture Research System of MOF and MARA (CARS-40), the Zhongyuan Youth Talent Support Program (ZYYCYU202012156), the Key Research Project of the Shennong Laboratory (SN01-2022-05) and Science and Technology Innovation Fund Project of Henan Agricultural University (KJCX2021A09).

Ethics Approval and Consent to Participate: All sample collection and treatment procedures were conducted in strict accordance with the ethical guidelines and protocol approved by the Institutional Animal Care and Use Committee (IACUC) of Henan Agricultural University, China (Permit Number: 11-0085; date: 13 June 2011). These measures were implemented to ensure animal welfare and minimize any potential suffering.

Consent for Publication: All authors read and approved the submitted version.

Data Availability Statement: The datasets supporting the conclusions of this article are included within the article and its additional files. Transcriptome sequencing data were deposited in the NCBI SRA database (SRA accession: PRJNA1031817).

DISCLOSURES

The authors declare no competing financial interests.

SUPPLEMENTARY MATERIALS

Supplementary material associated with this article can be found in the online version at doi:10.1016/j.psj.2024.103539.

REFERENCES

Agarwal, V., G. W. Bell, J. W. Nam, and D. P. Bartel. 2015. Predicting effective microRNA target sites in mammalian mRNAs. Elife 4:e05005.

Ala, U., F. A. Karreth, C. Bosia, A. Pagnani, R. Taulli, V. Léopold, Y. Tay, P. Provero, R. Zecchina, and P. P. Pandolfi. 2013. Integrated transcriptional and competitive endogenous RNA networks are cross-regulated in permissive molecular environments. Proc. Natl. Acad. Sci. USA. 110:7154–7159.

Chen, K., P. Manga, and S. J. Orlow. 2002. Pink-eyed dilution protein controls the processing of tyrosinase. Mol. Biol. Cell 13:1953–1964.

Conesa, A., S. Götz, J. M. García-Gómez, J. Terol, M. Talón, and M. Robles. 2005. Blast2GO: a universal tool for annotation, visualization and analysis in functional genomics research. Bioinformatics 21:3674–3676.

del Marmol, V., and F. Beermann. 1996. Tyrosinase and related proteins in mammalian pigmentation. FEBS Lett 381:165–168.

Dou, T., S. Yan, L. Liu, K. Wang, Z. Jian, Z. Xu, J. Zhao, Q. Wang, S. Sun, M. Z. Talpur, X. Duan, D. Gu, Y. He, Y. Du, A. M. Abdulwahid, Q. Li, H. Rong, W. Cao, Z. Su, G. Zhao, R. Liu, S. Zhao, Y. Huang, M. F. W. Te Pas, C. Ge, and J. Jia. 2022. Integrative analysis of transcriptomics and metabolomics to reveal the melanogenesis pathway of muscle and related meat characters in Wuliangshan black-boned chickens. BMC Genom 23:173.

Drögemüller, C., U. Philipp, B. Haase, A. R. Günzel-Apel, and T. Leeb. 2007. A noncoding melanophilin gene (MLPH) SNP at the splice donor of exon 1 represents a candidate causal mutation for coat color dilution in dogs. J. Hered 98:468–473.

Edwards, M., A. Bigham, J. Tan, S. Li, A. Gozdzik, K. Ross, L. Jin, and E. J. Parra. 2010. Association of the OCA2 polymorphism His615Arg with melanin content in east Asian populations: further evidence of convergent evolution of skin pigmentation. PLoS Genet 6:e1000867.

Frazee, A. C., G. Pertea, A. E. Jaffe, B. Langmead, S. L. Salzberg, and J. T. Leek. 2015. Ballgown bridges the gap between transcriptome assembly and expression analysis. Nat. Biotechnol 33:243–246.

Fu, X. Z., X. Y. Zhang, J. Y. Qiu, X. Zhou, M. Yuan, Y. Z. He, C. P. Chun, L. Cao, L. L. Ling, and L. Z. Peng. 2019. Whole-transcriptome RNA sequencing reveals the global molecular responses and ceRNA regulatory network of mRNAs, lncRNAs, miRNAs and circRNAs in response to copper toxicity in Ziyang Xiangcheng (Citrus junos Sieb. Ex Tanaka). BMC Plant Biol 19:509.

Guil, S., and M. Esteller. 2012. Cis-acting noncoding RNAs: friends and foes. Nature Struct. Mole. Biol. 19:1068–1075.

Haraszti, T., C. M. Trantow, A. Hedberg-Buenz, M. Grunze, and M. G. Anderson. 2011. Spectral analysis by XANES reveals that GPNMB influences the chemical composition of intact melanosomes. Pigment Cell Melanoma Res 24:187–196.

Houtgast, E. J., V. M. Sima, K. Bertels, and Z. Al-Ars. 2018. Hardware acceleration of BWA-MEM genomic short read mapping for longer read lengths. Comput. Biol. Chem 75:54–64.

Ishida, Y., V. A. David, E. Eizirik, A. A. Schäffer, B. A. Neelam, M. E. Roelke, S. S. Hannah, S. J. O'Brien, and M. Menotti-Raymond. 2006. A homozygous single-base deletion in MLPH causes the dilute coat color phenotype in the domestic cat. Genomics 88:698–705.

Jung, E., J. H. Kim, M. O. Kim, S. Jang, M. Kang, S. W. Oh, Y. H. Nho, S. H. Kang, M. H. Kim, S. H. Park, and J. Lee. 2016. Afzelin positively regulates melanogenesis through the p38 MAPK pathway. Chem. Biol. Interact 254:167–172.

Kanehisa, M., and S. Goto. 2000. KEGG: kyoto encyclopedia of genes and genomes. Nucleic Acids Res 28:27–30.

Kang, Y. J., D. C. Yang, L. Kong, M. Hou, Y. Q. Meng, L. Wei, and G. Gao. 2017. CPC2: a fast and accurate coding potential calculator based on sequence intrinsic features. Nucleic Acids Res 45: W12–W16.

Kechin, A., U. Boyarskikh, A. Kel, and M. Filipenko. 2017. cutPrimers: a new tool for accurate cutting of primers from reads of targeted next generation sequencing. J. Comput. Biol 24: 1138–1143.

Kim, D., G. Pertea, C. Trapnell, H. Pimentel, R. Kelley, and S. L. Salzberg. 2013. TopHat2: accurate alignment of

transcriptomes in the presence of insertions, deletions and gene fusions. Genome Biol 14:R36.
Kim, H. M., and C. G. Hyun. 2022. Miglitol, an oral antidiabetic drug, downregulates melanogenesis in B16F10 melanoma cells through the PKA, MAPK, and GSK3β/β-catenin signaling pathways. Molecules 28:115.
Langmead, B., and S. L. Salzberg. 2012. Fast gapped-read alignment with Bowtie 2. Nat. Methods 9:357–359.
Lee, S. W., J. M. Lim, H. Mohan, K. K. Seralathan, Y. J. Park, J. H. Lee, and B. T. Oh. 2020. Enhanced bioactivity of Zanthoxylum schinifolium fermented extract: anti-inflammatory, anti-bacterial, and anti-melanogenic activity. J. Biosci. Bioeng 129:638–645.
Li, D., G. Sun, M. Zhang, Y. Cao, C. Zhang, Y. Fu, F. Li, G. Li, R. Jiang, R. Han, Z. Li, Y. Wang, Y. Tian, X. Liu, W. Li, and X. Kang. 2020. Breeding history and candidate genes responsible for black skin of Xichuan black-bone chicken. BMC Genom 21:511.
Li, D., X. Wang, Y. Fu, C. Zhang, Y. Cao, J. Wang, Y. Zhang, Y. Li, Y. Chen, Z. Li, W. Li, R. Jiang, G. Sun, Y. Tian, G. Li, and X. Kang. 2019. Transcriptome analysis of the breast muscle of Xichuan black-bone chickens under tyrosine supplementation revealed the mechanism of tyrosine-induced melanin deposition. Front. Genet 10:457.
Li, H., L. Fan, S. Zhu, M. K. Shin, F. Lu, J. Qu, and L. Hou. 2017. Epilation induces hair and skin pigmentation through an EDN3/EDNRB-dependent regenerative response of melanocyte stem cells. Sci. Rep 7:7272.
Lin, L.-C., and W.-T. Chen. 2005. The study of antioxidant effects in melanins extracted from various tissues of animals. Asian-Australas J. Anim. Sci 18:277–281.
Ma, M., B. Cai, L. Jiang, B. A. Abdalla, Z. Li, Q. Nie, and X. Zhang. 2018. lncRNA-Six1 Is a Target of miR-1611 that functions as a ceRNA to regulate six1 protein expression and fiber type switching in chicken myogenesis. Cells 7:12.
Makpol, S., F. A. Jam, N. A. Rahim, S. C. Khor, Z. Ismail, Y. A. Yusof, and W. Z. Wan Ngah. 2014. Comparable down-regulation of TYR, TYRP1 and TYRP2 genes and inhibition of melanogenesis by tyrostat, tocotrienol-rich fraction and tocopherol in human skin melanocytes improves skin pigmentation. Clin. Ter 165:e39–e45.
Myung, C. H., J. E. Lee, C. S. Jo, J. I. Park, and J. S. Hwang. 2021. Regulation of Melanophilin (Mlph) gene expression by the glucocorticoid receptor (GR). Sci. Rep 11:16813.
Ng, A., R. A. Uribe, L. Yieh, R. Nuckels, and J. M. Gross. 2009. Zebrafish mutations in gart and paics identify crucial roles for de novo purine synthesis in vertebrate pigmentation and ocular development. Development 136:2601–2611.
Pak, B. J., J. Lee, B. L. Thai, S. Y. Fuchs, Y. Shaked, Z. Ronai, R. S. Kerbel, and Y. Ben-David. 2004. Radiation resistance of human melanoma analysed by retroviral insertional mutagenesis reveals a possible role for dopachrome tautomerase. Oncogene 23:30–38.
Park, J. S., J. H. Ryu, T. I. Choi, Y. K. Bae, S. Lee, H. J. Kang, and C. H. Kim. 2016. Innate color preference of zebrafish and its use in behavioral analyses. Mol. Cells 39:750–755.
Paterson, E. K., T. J. Fielder, G. R. MacGregor, S. Ito, K. Wakamatsu, D. L. Gillen, V. Eby, R. E. Boissy, and A. K. Ganesan. 2015. Tyrosinase depletion prevents the maturation of melanosomes in the mouse hair follicle. PLoS One 10: e0143702.
Pertea, M., G. M. Pertea, C. M. Antonescu, T. C. Chang, J. T. Mendell, and S. L. Salzberg. 2015. StringTie enables improved reconstruction of a transcriptome from RNA-seq reads. Nat. Biotechnol 33:290–295.
Philipp, U., H. Hamann, L. Mecklenburg, S. Nishino, E. Mignot, A. R. Günzel-Apel, S. M. Schmutz, and T. Leeb. 2005. Polymorphisms within the canine MLPH gene are associated with dilute coat color in dogs. BMC Genet 6:34.
Pillaiyar, T., M. Manickam, and S. H. Jung. 2017. Recent development of signaling pathways inhibitors of melanogenesis. Cell Signal 40:99–115.
Pralea, I. E., R. C. Moldovan, A. M. Petrache, M. Ilieş, S. C. Hegheş, I. Ielciu, R. Nicoară, M. Moldovan, M. Ene, M. Radu, A. Uifălean, and C. A. Iuga. 2019. From Extraction to advanced analytical methods: the challenges of melanin analysis. Int. J. Mol. Sci 20:16.
Protas, M. E., C. Hersey, D. Kochanek, Y. Zhou, H. Wilkens, W. R. Jeffery, L. I. Zon, R. Borowsky, and C. J. Tabin. 2006. Genetic analysis of cavefish reveals molecular convergence in the evolution of albinism. Nat. Genet 38:107–111.
Rosemblat, S., D. Durham-Pierre, J. M. Gardner, Y. Nakatsu, M. H. Brilliant, and S. J. Orlow. 1994. Identification of a melanosomal membrane protein encoded by the pink-eyed dilution (type II oculocutaneous albinism) gene. Proc. Natl. Acad. Sci. USA. 91:12071–12075.
Salmena, L., L. Poliseno, Y. Tay, L. Kats, and P. P. Pandolfi. 2011. A ceRNA hypothesis: the Rosetta Stone of a hidden RNA language? Cell 146:353–358.
Schiaffino, M. V. 2010. Signaling pathways in melanosome biogenesis and pathology. Int J Biochem Cell Biol 42:1094–1104.
Shannon, P., A. Markiel, O. Ozier, N. S. Baliga, J. T. Wang, D. Ramage, N. Amin, B. Schwikowski, and T. Ideker. 2003. Cytoscape: a software environment for integrated models of biomolecular interaction networks. Genome Res 13:2498–2504.
Shao, L. L., X. L. Wang, K. Chen, X. W. Dong, L. M. Kong, D. Y. Zhao, R. C. Hider, and T. Zhou. 2018. Novel hydroxypyridinone derivatives containing an oxime ether moiety: Synthesis, inhibition on mushroom tyrosinase and application in anti-browning of fresh-cut apples. Food Chem 242:174–181.
Stokowski, R. P., P. V. Pant, T. Dadd, A. Fereday, D. A. Hinds, C. Jarman, W. Filsell, R. S. Ginger, M. R. Green, F. J. van der Ouderaa, and D. R. Cox. 2007. A genomewide association study of skin pigmentation in a South Asian population. Am. J. Hum. Genet 81:1119–1132.
Sun, L., H. Luo, D. Bu, G. Zhao, K. Yu, C. Zhang, Y. Liu, R. Chen, and Y. Zhao. 2013. Utilizing sequence intrinsic composition to classify protein-coding and long non-coding transcripts. Nucleic Acids Res 41:e166.
Takeo, M., W. Lee, P. Rabbani, Q. Sun, H. Hu, C. H. Lim, P. Manga, and M. Ito. 2016. EdnrB governs regenerative response of melanocyte stem cells by crosstalk with Wnt signaling. Cell Rep 15:1291–1302.
Tian, Y., M. Xie, W. Wang, H. Wu, Z. Fu, and L. Lin. 2007. Determination of carnosine in Black-Bone Silky Fowl (Gallus gallus domesticus Brisson) and common chicken by HPLC. Eur. Food Res. Technol 226:311–314.
Tímár, J., L. Mészáros, A. Ladányi, L. G. Puskás, and E. Rásó. 2006. Melanoma genomics reveals signatures of sensitivity to bio- and targeted therapies. Cell Immunol 244:154–157.
Toyofuku, K., J. C. Valencia, T. Kushimoto, G. E. Costin, V. M. Virador, W. D. Vieira, V. J. Ferrans, and V. J. Hearing. 2002. The etiology of oculocutaneous albinism (OCA) type II: the pink protein modulates the processing and transport of tyrosinase. Pigment Cell Res 15:217–224.
Tu, Y.-g., Y.-z. Sun, Y.-g. Tian, M.-y. Xie, and J. Chen. 2009. Physicochemical characterisation and antioxidant activity of melanin from the muscles of Taihe Black-bone silky fowl (Gallus gallus domesticus Brisson). Food Chem. 114:1345–1350.
Wang, L., H. Liu, B. Hu, J. Hu, H. Xu, H. He, C. Han, B. Kang, L. Bai, R. Zhang, J. Wang, S. Hu, and L. Li. 2021. Transcriptome reveals genes involving in black skin color formation of ducks. Genes Genom. 43:173–182.
Wang, W., Q. Shi, S. Wang, H. Zhang, and S. Xu. 2020. Ammonia regulates chicken tracheal cell necroptosis via the LncRNA-107053293/MiR-148a-3p/FAF1 axis. J Hazard Mater 386:121626.
Wu, P. Y., Y. J. You, Y. J. Liu, C. W. Hou, C. S. Wu, K. C. Wen, C. Y. Lin, and H. M. Chiang. 2018. Sesamol inhibited melanogenesis by regulating melanin-related signal transduction in B16F10 cells. Int J Mol Sci 19:4.
Xiong, Q., H. Tao, N. Zhang, L. Zhang, G. Wang, X. Li, X. Suo, F. Zhang, Y. Liu, and M. Chen. 2020. Skin transcriptome profiles associated with black- and white-coated regions in Boer and Macheng black crossbred goats. Genomics 112:1853–1860.
Yang, C. W., J. S. Ran, C. L. Yu, M. H. Qiu, Z. R. Zhang, H. R. Du, Q. Y. Li, X. Xiong, X. Y. Song, B. Xia, C. M. Hu, Y. P. Liu, and X. S. Jiang. 2019. Polymorphism in MC1R, TYR and ASIP genes in different colored feather chickens. 3 Biotech 9:203.
Yu, F., Y. Lu, Z. Zhong, B. Qu, M. Wang, X. Yu, and J. Chen. 2021. Mitf involved in innate immunity by activating tyrosinase-mediated melanin synthesis in Pteria penguin. Front. Immunol 12:626493.

Yu, S., G. Wang, J. Liao, and M. Tang. 2018. Transcriptome profile analysis identifies candidate genes for the melanin pigmentation of breast muscle in Muchuan black-boned chicken. Poult Sci 97:3446–3455.

Yuan, H., X. Zhang, Q. Zhang, Y. Wang, S. Wang, Y. Li, Y. Zhang, J. Jing, J. Qiu, Z. Wang, and L. Leng. 2019. Comparative transcriptome profiles of Lindian chicken eyelids identify melanin genes controlling eyelid pigmentation. Br. Poult. Sci 60:15–22.

Zi, X., X. Ge, Y. Zhu, Y. Liu, D. Sun, Z. Li, M. Liu, Z. You, B. Wang, and J. Kang. 2023. Transcriptome profile analysis identifies candidate genes for the melanin pigmentation of skin in tengchong snow chickens. Vet. Sci. 10:341.